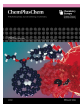

An Androsterone-H_2@C_{60} hybrid: Synthesis, Properties and Molecular Docking Simulations with SARS-Cov-2

Margarita Suárez,*[a] Kamil Makowski,[b] Reinier Lemos,[a] Luis Almagro,[a] Hortensia Rodríguez,[c] María Ángeles Herranz,[d] Dolores Molero,[e] Orlando Ortiz,[a] Enrique Maroto,[d] Fernando Albericio,[f] Yasujiro Murata,[g] and Nazario Martín*[d]

We report the synthesis and characterization of a fullerene-steroid hybrid that contains H_2@C_{60} and a dehydroepiandrosterone moiety synthesized by a cyclopropanation reaction with 76% yield. Theoretical calculations at the DFT-D3(BJ)/PBE 6-311G(d,p) level predict the most stable conformation and that the saturation of a double bond is the main factor causing the upfield shielding of the signal appearing at −3.13 ppm, which corresponds to the H_2 located inside the fullerene cage. Relevant stereoelectronic parameters were also investigated and reinforce the idea that electronic interactions must be considered to develop studies on chemical-biological interactions. A molecular docking simulation predicted that the binding energy values for the protease-hybrid complexes were −9.9 kcal/mol and −13.5 kcal/mol for PL^{pro} and $3CL^{pro}$ respectively, indicating the potential use of the synthesized steroid-H_2@C_{60} as anti-SARS-Cov-2 agent.

Introduction

It is widely known that endohedral fullerenes can provide novel ball-shaped molecules with exceptional structures and physical properties, which are unobserved for their empty analogs. Therefore, the encapsulation of different atoms or molecules, such as water,[1] metal atoms,[2] or trimetallic nitride clusters[3] within the fullerene cavity has attracted wide interest from researchers worldwide. In this regard, the development of synthetic protocols has allowed to synthesizing several endohedral fullerenes, which have shown a practical application either in biomedicine[4,5] or materials science.[6,7]

A groundbreaking synthetic methodology coined the "molecular surgery" approach[8] was developed by Komatsu, Murata and co-workers in 2003.[9] This new approach resulted in the synthesis on an open-cage derivative with 100% incorporation of H_2 molecule into the fullerene cage. In this sense, different chemical methods have been reported to convert open-cage fullerenes into endohedric derivatives and to produce H_2@C_{60} in milligram amounts.[10] A most recent high-yielding synthetic methodology to obtain H_2@C_{60} was described by Whitby *et al.*,[11] and these results have paved the way for the advancement in fundamental as well as applied studies on this singular molecule.

As yet, H_2@C_{60} is among the most studied small-molecule endofullerene.[12] Most of the research reported focused on the study of its physical properties. In this way, techniques such as IR,[13] NMR,[14] and photoionization[15] have been used to explain the interactions between the molecular hydrogen and the carbon cage surface. Moreover, theoretical calculations have allowed the prediction of some parameters that have led to a better understanding of hydrogen-filled endohedral fullerene complexes.[16]

The cycloaddition reactions of H_2@C_{60} to yield methanofullerene and fulleropyrrolidine adducts have been reported to investigate potential changes on the reactivity of the outer fullerene cage due to the encapsulated hydrogen.[17] Besides, a small library of H_2@C_{60} derivatives covalently linked to a nitroxide radical have been prepared using either Prato or Bingel-Hirsh methodologies.[18,19] Moreover, similar derivatives, in which a nitroxide radical is connected to the endofullerene by a folded 3_{10}-helical peptide,[20] and also bisadduct isomers of a H_2@C_{60} derivative modified with nitroxide appendages have also been reported.[21]

[a] Prof. Dr. M. Suárez, R. Lemos, L. Almagro, O. Ortiz
Laboratorio de Síntesis Orgánica
Facultad de Química
Universidad de la Habana
10400 La Habana (Cuba)
E-mail: msuarez@fq.uh.cu
Homepage: http://www.fq.uh.cu
[b] Dr. K. Makowski
Departament of Surfactants and Nanobiotechnology
Institute for Advanced Chemistry of Catalonia (IQAC-CSIC) and CIBER-BBN
Barcelona (Spain)
[c] Dr. H. Rodríguez
Yachay Tech University
School of Chemical Sciences and Engineering
100119-Urququi (Ecuador)
[d] Dr. M. Á. Herranz, Dr. E. Maroto, Prof. Dr. N. Martín
Departamento de Química Orgánica
Facultad de Ciencias Químicas
Universidad Complutense de Madrid
28040-Madrid (Spain)
E-mail: nazmar@ucm.es
Homepage: http://www.nazariomartingroup.com
[e] Dr. D. Molero
CAI RMN Universidad Complutense de Madrid
28040 Madrid (Spain)
[f] Prof. Dr. F. Albericio
School of Chemistry and Physics
University of KwaZul-Natal
Durban (South Africa)
[g] Prof. Dr. Y. Murata
Institute for Chemical Research
Kyoto University
Uji, Kyoto, 611-0011 (Japan)

Supporting information for this article is available on the WWW under https://doi.org/10.1002/cplu.202000770

In addition, the stereoselective synthesis of $H_2@C_{60}$, was first described by Martín and co-workers, reacting chiral ligands and metal salts through a 1,3-dipolar cycloaddition reaction of azomethine ylides.[22] Thus, an interesting finding regarding the encapsulation of a hydrogen molecule is that the process itself does not affect the reactivity or the stereoselectivity, as the observed results are similar to those of the hollow fullerene C_{60}.[23]

Interestingly, studies carried out by Turro *et al.* revealed that, actually, a crucial electron and vibrational interaction of incarcerated H_2 in endofullerene $H_2@C_{60}$ with an external electronically excited molecule like singlet oxygen occurs.[24] Therefore, endohedral fullerenes could be used as probes for further experimental studies and, in this regard, much works remains to be done to developed new $H_2@C_{60}$ derivatives. In particular, there is still much research to be done to develop novel synthetic procedures to generate $H_2@C_{60}$ derivatives suitable for biological investigations.

In this sense, during the last decade our research groups have carried out considerable experimental and theoretical work on novel steroid-fullerene hybrids for fundamental studies and their potential applications in diverse fields like medicinal chemistry and materials science.[25]

To the best of our knowledge, there are not reports where the $H_2@C_{60}$ is conjugated with a steroid moiety. Hence, herein, we describe the synthetic methodology to access a new conjugate where the endohedral fullerene, $H_2@C_{60}$, is covalently attached to the dehydroepiandrosterone (DHEA), a naturally occurring steroid, which presents interesting bioactive properties.[26] To achieve this goal, the Bingel-Hirsh methodology was used.[27] This synthetic procedure constitutes one of the most widely applied reactions in fullerene's chemistry, due to its good selectivity and feasibility of adding a wide range of addends and functional groups.

The chemical structure of the as-synthesized steroid-$H_2@C_{60}$ was unambiguously corroborated by NMR (1D and 2D), IR, and mass spectrometry. Furthermore, theoretical calculations were achieved to envision the most stable conformation for the prepared compound, as well as to evaluate other relevant physico-chemical characteristics such as polarity, polarizability, and lipophilicity. Finally, a molecular docking simulation was carried out to predict the use of the synthesized steroid-$H_2@C_{60}$ as potential inhibitor of SARS-Cov-2, proteases $3CL^{pro}$[28] and PL^{pro},[29] two of the enzymes that play crucial roles in the viral life cycle of the 2019 novel coronavirus or "2019-nCoV",[30] and constitute important targets for antiviral drug design.

Results and Discussion

The novel steroid-endohedral fullerene hybrid **3** was synthesized through the cycloaddition reaction between the previously reported 3β-ethyl malonate-5-androsten-17-one (**1**)[31] and $H_2@C_{60}$, using a Bingel-Hirsch methodology, as depicted in Scheme 1.

The cyclopropanation reaction was carried out at room temperature by mixing the $H_2@[60]$fullerene with **1**, CBr_4 and DBU (see Scheme 1). Right after the DBU addition a change in the color of the solution from purple to brown was observed, which is a similar color change to that observed when the reaction is performed using the pristine C_{60}.[31] In this regard, according to our previous studies a change in the coloration of the solution constitutes an evidence of chemical transformation onto the [60]fullerene molecule, which leads to a [6,6]-closed mono-adduct. The reaction was followed by thin-layer chromatography (TLC), proceeding apace, since after 3 h it was completed. Then, the synthesized conjugate **3** was purified by flash chromatography, being firstly eluted the unreacted $H_2@C_{60}$ using CS_2, followed by the elution of the mono-adduct **3**, with DCM as solvent. The endohedral hybrid was separated as a stable brown solid with a 76% yield. The reaction mixture was investigated by HPLC, observing in the chromatogram (toluene: acetonitrile, 9:1, 1 mL min^{-1}) a peak at 5.5 min, assigned to hybrid molecule **3** (see Figure S10 in the Supporting Information), and a peak at 8.9 min corresponding to the unreacted $H_2@C_{60}$.

It should be noticed that the reaction rate and the obtained yield are near to the same values disclosed for the functionalization of the hollow [60]fullerene with steroids.[25a,25e,31] Thus, the H_2 molecule trapped inside the fullerene cavity does not influences the fullerene's cage reactivity as it was previously established.[22]

The structural elucidation of the as-synthesized steroid-endohedral fullerene **3** was accomplished using different spectroscopic techniques (see Experimental Section and Supporting Information). In this respect, FTIR spectrum exhibited

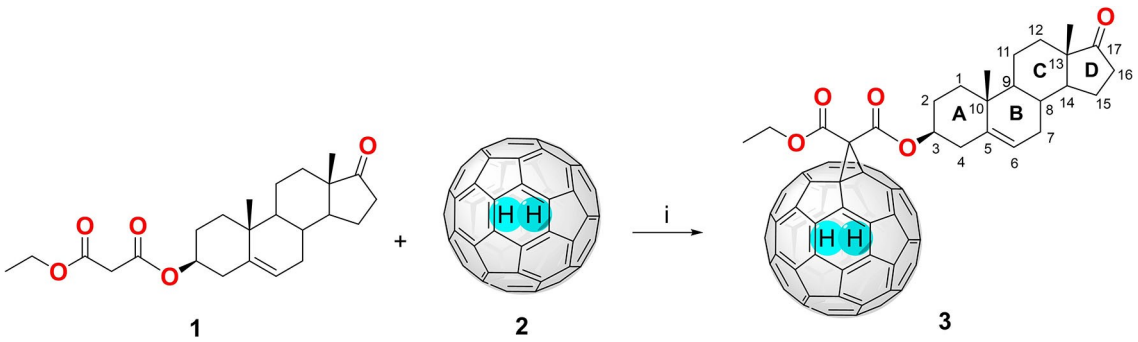

1 2 3

Scheme 1. Synthesis of hybrid steroid-$H_2@C_{60}$. i) CBr_4, DBU, toluene, room temperature.

the specific band of organofullerene derivatives at ca. 730 cm^{-1},[32] and a signal at 1720 cm^{-1} corresponding to the C=O stretching vibration (see Figure S8 in the Supporting Information).

NMR spectroscopy was used to substantiate the covalent link of the malonate-steroid to the $H_2@C_{60}$ sphere. Thus, in the ^{1}H NMR spectra, the methylene protons of the malonate-steroid precursor at $\delta = 3.33$ ppm were not observed, and two signals at 1.51 ppm and 4.58 ppm, were assigned to the protons of the ethoxycarbonyl group. Moreover, the presence of a doublet at $\delta = 5.52$ ppm assigned to the proton H6 of the ring B and the proton on C3 positioned at ring A, at $\delta = 5.03$ ppm, indicate the existence of the steroid fragment in the conjugate. Furthermore, due to the $H_2@C_{60}$ cage, these signals are deshielded related to their positions in the precursor **1**, at 5.34 ppm and 4.59 ppm, respectively.[31] Therefore, these signals confirmed the proposed structure of the steroid-endohedral hybrid **3**. In addition, in the ^{1}H NMR spectrum is particularly remarkable the presence of a singlet at $\delta = -3.13$ ppm that corresponds to the encapsulated hydrogen molecule. Interestingly, this signal appears at a higher field than the value reported for $H_2@C_{60}$ ($\delta = -1.45$ ppm).[19] In order to find the reasons behind this change in the chemical shift, we theoretically estimated the chemical shifts for compounds **3**, a $H_2@C_{60}$-cyclopropane, and $H_2@C_{60}$ (see Table S1 in the Supporting Information for details). The results showed that the saturation of a double bond is the main factor causing the upfield shielding of the H_2 located inside the fullerene cage, since the calculated upfield shift of the molecular hydrogen from $H_2@C_{60}$ to $H_2@C_{60}$-cyclopropane is 2.77 ppm, only 0.83 less than for compound **3**. These results are in agreement with the chemical shift change sensitivity reported for different derivatives of $H_2@C_{60}$, and in particular with the value of −3.27 ppm reported for the Bingel-Hirsch cycloadduct formed by $H_2@C_{60}$ and diethylmalonate.[10b] Additionally, the hydrogen molecule is slightly off-center displaced in **3** when compared to $H_2@C_{60}$, but this might only marginally impact the magnetic environment of the hydrogen (Figure S12).

^{13}C NMR confirmed the formation of a monoadduct in the reaction of $H_2@C_{60}$ with **1**. In this regard, due to the lack of symmetry of the endohedral derivative **3** an increment in the number of signals between 145.4–139.4 ppm was observed. Moreover, two signals at 163.8 and 163.1 ppm were assigned to the two carbonyl groups present in the malonate fragment, which helped to corroborate the proposed structure of hybrid **3**. In addition, the presence of the steroid motif was confirmed by a signal at low field (221.2 ppm) assigned to the C=O located at the C17 of the steroid backbone. Besides, the signals corresponding to C5, C6, and C3 of the steroid motif at 139.2, 122.9, and 77.4 ppm, respectively, were also detected, being the latter signal strongly deshielded by ca. 2 ppm, compared to the same signal in compound **1**, due to the presence of the carbon sphere.

Furthermore, the other signals of the steroid scaffold were not affected by the presence of the $H_2@C_{60}$ cage (see Experimental Section). Finally, the signals associated with the sp^3 carbon atoms of the cyclopropane ring at the 6,6-ring juncture of the $H_2@C_{60}$ structure were detected at $\delta = 72.7$ and 71.8 ppm. The signals of quaternary carbon atoms appeared at 52.5 ppm.

HSQC spectra have allowed straightforwardly the assignment of the ^{1}H NMR and ^{13}C NMR. In this sense, the analysis was based on the chemical shift's theory, substituent effects, and DEPT data. The assignment of quaternary carbon atoms was carried out through the analysis of the HMBC spectra. Furthermore, it is worth noting that **3** showed similar trends in the chemical shifts of the molecular backbone to those of **1**, which constitute an evidence of the proposed chemical structure for the novel steroid-endohedral fullerene (see Experimental Section and Supporting Information)

The proposed structure was verified by Mass Spectrometry. Consequently, the MALDI-TOF spectra of compound **3** showed a peak at *m/z*: 1122.2399 (calculated for $C_{84}H_{34}O_5$: 1122.2406) corresponding to M^+ ion (See Figure S9). Furthermore, Figure S11 in the Supporting Information shows the UV-vis spectra of **3**, which exhibit the classical profile of fullerene derivatives, showing a band centered at 430 nm as a representative identification for [6,6]-closed fullerene monoadducts.[33]

A finding of paramount importance for future biological applications relies on the increment of solubility in organic solvents, such as chloroform, dichloromethane, dimethylsulfoxide, and dimethylformamide, underwent by the hybrid **3** when compared with the parent $H_2@C_{60}$. This enhancement is directly related to the presence of polar groups on the steroid motif.

The geometrical and electronic properties of the as-synthesized hybrid **3** have been calculated. In this sense, we developed a theoretical study using density functional theory (DFT). In a first place, the molecule was pre-optimized with PM6-D3H4 semiempirical method as a useful starting point for further calculations.[34] For DFT calculations, the PBE functional was used as it showed good results in carbon systems as fullerenes,[35] and in endohedral fullerene systems,[36,37] together with a reasonable computational cost, especially for the frequency calculations needed to assure getting the minimum energy conformations. Furthermore, it should be considered that in the endohedral system with nonpolar molecules as H_2 the London dispersion forces became very important to take into account.[38] Therefore, the third version of dispersion correction, together with Becke-Johnson damping (D3BJ) was applied.[39] The first structure optimization was carried out with 6-31G(d) basis set and then after triple zeta 6-311G(d,p) was used to reassure good quality results. The minimum energy conformation of compound **3** is depicted in Figure 1.

The total energies calculated using PM6 and DFT (Table S7) along with the Cartesian atom coordinates (Tables S2–S6) are given in the Supporting Information. Moreover, the overlap structures which were optimized by PM6-D3H4 and DFT PBE-D3BJ 6-311G(d,p) are shown in Figure S13.

The calculations have predicted the cyclohexane ring A of the steroid moiety to present a chair conformation. Furthermore, the carbonyl groups in the malonate moiety in the DFT-D3 optimized structure present an antiperiplanar disposition with a dihedral O=C···C=O angle of −161.2°. This atoms disposition does not permit the formation of a hydrogen bond

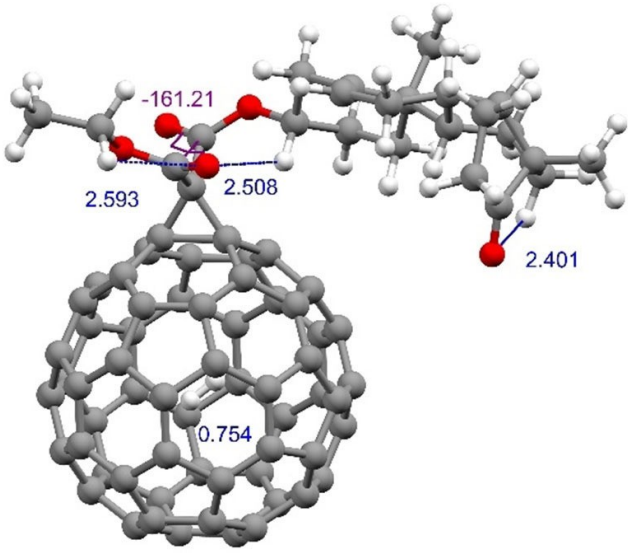

Figure 1. Minimum energy conformation of compounds **3** obtained by the DFT–D3(BJ) method at the PBE/6-311G(d,p) level of theory Bond distances are given in Å and dihedral angle in degree °.

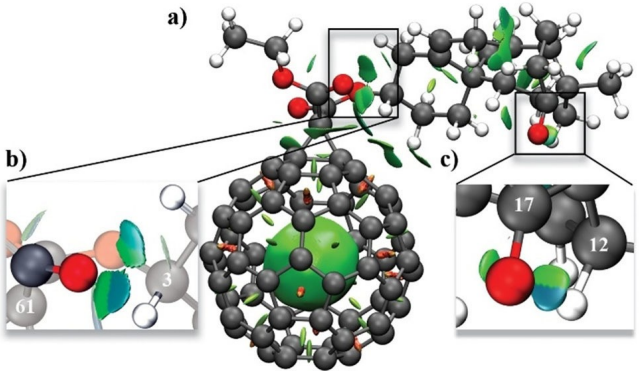

Figure 2. Non-covalent interactions (NCI) analysis of compound **3** in the gas phase. Isosurfaces represent the regions of interactions where green represents weak van der Waals interactions, blue strong attractive interactions and red strong repulsive interactions. For a better visualization an arrow focuses on interactions near to the A-ring (2b) and near to the D-ring (2c) of the steroid scaffold.

between H3 and the oxygen from the closest carbonyl group. However, H3 forms hydrogen bond with the other carbonyl with a C=O···H distance of 2.51 Å. In addition, this carbonyl group participates in another interaction with the methylene hydrogen atom (2.59 Å). Interestingly, ring C presents a twisted boat conformation that can be the result of the hydrogen bond formed between the carbonyl from the cyclopentanone ring and the β-hydrogen join to the C12 on C ring of the steroid backbone (2.401 Å) (Figure 1). Regarding the disposition of the inner hydrogen molecule, Korona *et al.*[40] performed the analysis of the disposition of H_2 in a different not fully optimized structure of conformers of $H_2@C_{60}$. The conformation is energetically favored when the hydrogen molecule is perpendicular to one of the hexagonal rings. In the case of the hybrid steroid-$H_2@C_{60}$, the optimized structure does not present orientation in a clear perpendicular position of hydrogen molecule to any of the hexagonal rings (Figure S14 in the Supporting Information). Similar results were found by Cross[41] who studied the rotational movement of the encapsulated H_2 and reported a free motion of the H_2 molecule inside C_{60}.

In addition, a Non-Covalent Interactions (NCI) analysis was performed, following the approach proposed by Johnson et al.[42] using the NCIPLOT program.[43] These results confirmed the presence of hydrogen bonding (Figure 2, greenish color) between the oxygen atom located at C17 of the ring D and H12 (Figure 2c), those formed among the oxygen atoms of the malonate moiety with H3 (Figure 2b), and one of the hydrogens of the methylene group (upper left part of Figure 2a).

On the other hand, DFT combined with symmetry-adapted perturbation theory (SAPT) calculation of endohedral $H_2@C_{60}$ by Korona et al.[40] showed there is a weak stabilization interaction of the complex between the fullerene carbon cage and the H_2 guest molecule with a value of −19.35 kJ/mol. The stabilization energy calculated by the supermolecule approach for $H_2@C_{60}$ was carried out by Ramachandran *et al.*[44] at MP2/6-31G level of theory using the following equation $\Delta E_{stab} = E_{complex} - (E_{cage} + E_{guest})$ gives −2.1 kcal/mol. Using the same approach at DFT-D3(BJ)/PBE/6-311G(d,p) level, the stabilization energy for compound **3** was found to be −6.43 kcal/mol. Additionally, the NCI analysis confirmed the presence of hydrogen bonding (bluish color) between the oxygen atom located at C17 of the ring D and H12 (Figure 2c) those formed among the oxygen atoms of the malonate moiety with H3 and one of the hydrogens of the methylene of the ethyl group (Figure 2b).

Additionally, the LUMO-HOMO energy values predicted by DFT calculation at PBE-D3JP/6-311G(d,p) level of theory are −4.081 eV/−5.414 eV. A band gap of 1.332 eV has been predicted. This value is quite similar to experimental values determined in analogous compounds.[25f,31] (See Figure S15 in the Supporting Information).

In addition, to predict the intramolecular and intermolecular electrostatic interactions in hybrid **3**, the molecular electrostatic potential map and selected descriptors and properties were calculated. Also, the same parameters were calculated for the pristine endohedral $H_2@C_{60}$.

The electrostatic potential maps of **3** and $H_2@C_{60}$ are depicted in Figure 3. From its analysis, it is possible to conclude that the malonate-steroid core, covalently connected to the $H_2@C_{60}$ cage, modifies the electrostatic potential distribution providing three well-defined regions. In this sense, the red zone was correlated with the oxygen atoms present in the carbonyl groups and denoted a negative density site. The regions with blue color indicate the positive areas located in some part of the steroid skeleton. Furthermore, a significant part of the molecular hybrid showed neutral green regions predicting no charge separation, indicating the lipophilicity of the molecule. On the other hand, a comparison with the electrostatic potential map of the corresponding derivative without the H_2 molecule inside the fullerene cage, previously reported by our research groups,[31] allowed to conclude that the H_2 molecule present in the endohedral derivative, does not influence the

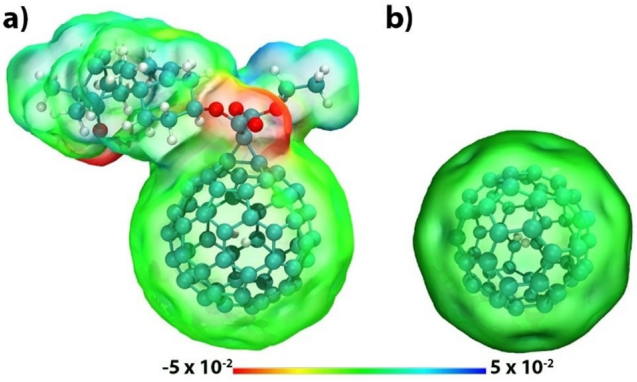

Figure 3. Depiction of the molecular electrostatic potential maps for the optimized functionalized endohedral fullerene **3** (a) and $H_2@C_{60}$ (b). The red color, represented negative potential, blue color the positive potential and green color the uncharged regions.

electronic properties of the different functional groups present in the $H_2@C_{60}$ derivative.

Additional properties were calculated for **3**, and compared with those related to $H_2@C_{60}$ (Table 1). All results are consistent with the structural analysis of both compounds.

The solvent-accessible surface area (SASA) is a geometric measure of the extent to which a molecule interacts with its environment. The transformation of $H_2@C_{60}$ to hybrid steroid-$H_2@C_{60}$ (**3**) leads to an increase in this parameter, which can be interpreted as a higher probability of interaction of **3** with targets of interest. The variation of SASA has also been used as an indirect confirmation of the capacity of C_{60} as a K^+ channel blocker.[49]

Related to the topological polar surface area (TPSA), which is a descriptor defined as the sum of surfaces of polar atoms in a molecule, Palm *et al.*[50] found a correlation between TPSA value and its ability to penetrate biological membranes, demonstrating that those molecules with a TPSA lower than 60 Å^2 are easily absorbed, and molecules with TPSA values greater than 140 Å^2 could have a low capacity for penetrating cell membranes It may account for their ready penetration capability in hydrophilic environments. As expected, the calculated TPSA was 0 for $H_2@C_{60}$, while for the hybrid steroid-$H_2@C_{60}$ (**3**) was 69.67 Å^2 a value very close to set threshold of 60 Å^2. These results are consistent with the covalent linking to the $H_2@C_{60}$ structures of the malonate-steroid moiety, conferring some polarity to the surface of molecular hybrid **3** in comparison with the highly hydrophobic $H_2@C_{60}$. Therefore, **3** may act as potential biological membrane spanners.

Table 1. Theoretical physicochemical parameters calculated for **3** and $H_2@C_{60}$.

Property	Compound **3**	$H_2@C_{60}$
Volume [Å][a]	879.1	532.9
SASA [Å^2] [b]	968.64	552.68
TPSA [Å^2] [c]	69.67	0.0
Hy[d]	−6.007	−5.762
Dipole moment [D][e]	5.45	0.002
logP[f]	11.96	17.75
Polarizability [Å^3][g]	811.95	511.79

[a] Total volume calculated in Chimera 1.14 using MSMS library for surface generation.[45] [b] Solvent-accessible surface area calculated by FreeSASA 2.0.3 with Lee and Richards algorithm.[46] [c] Topological polar surface area calculated by BioTriangle web server.[47] [d] Hydrophilic index calculated by BioTriangle web server.[47] [e] Dipole moment retrieved from DFT calculation. [f] Predicted octanol/water partition coefficient (lipophilicity) using XLOGP2v3.2.0.[48] [g] Polarizability predicted with single point energy calculation using PBE functional and 6-311G(d,p) basis set.

As expected for a structure only formed by carbon atoms, [60]fullerene has been considered to be hyperhydrophobic.[51,52] The partition coefficient (P) is a physicochemical parameter, which allows determining the lipophilicity degree of **3** and $H_2@C_{60}$ molecules. Thus, P could be defined as a quantitative parameter that represents the relative solubility of a given substance in a system composed of two phases that are immiscible with each other, at a specific temperature.

The $logP_{ow}$ obtained through theoretical calculations showed that both compounds have high lipophilicity, but a lower value for **3** (11.96) in comparison with $H_2@C_{60}$ (17.75) indicative of a lower hydrophobicity, which is consistent with the presence of the malonate-steroid moiety. These values might indicate that this kind of molecules would have the tendency to form aggregates in aqueous media, similar to the behavior reported for C_{60} and their derivatives.[53–55]

On the other hand, although $H_2@C_{60}$-steroid conjugation produced a weak charge separation as observed in Figure 3a, for compound **3** a calculated dipole moment of 5.45 D was predicted.

Thus, in comparison with pristine **2** (Figure 3b), a notably enlarged polarizability was observed (811.95 Å^3 vs. 511.79 Å^3). In this respect, polarizability displays a key role in determining induction and dispersion forces in molecules. Besides, atomic polarizabilities are widely used both in qualitative schemes for rationalizing molecular interactions as well as in quantitative techniques for modelling purposes. On the other hand, and according to the quenched polarizability model,[56] the polarizability of C_{60} does not change significantly by the encapsulation of atoms or small molecules. Overall, the structural modification incorporated in the endohedral derivative **3** corresponds to a higher value of polarizability, in comparison with $H_2@C_{60}$. All these results reinforce the idea that electronic interactions must be considered to develop studies on chemical-biological interactions.

The applications of the novel steroid-endohedral fullerene hybrid were also evaluated in medicinal chemistry, in particular, was explored its potential as antiviral at a theoretical level. Molecular docking of the steroid-$H_2@C_{60}$ (**3**) was performed. The molecular targets studied here were the papain-like protease (PL^{pro}) [PDB ID: 4OVZ with 2.50 Å resolution, chain A][57] and the 3-chymotrypsin-like protease ($3CL^{pro}$) [PDB ID: 6LU7 with 2.02 Å resolution) chain A)][58] of SARS-Cov-2. These are cysteine proteases that play crucial roles in the viral life cycle and are key targets for antiviral drug design.[59]

The calculated negative binding energy[60] predicted that compound **3** has affinity for both enzymes. The binding energy values for the protease-hybrid complexes were −9.9 kcal/mol and −13.5 kcal/mol for PL^{pro} and $3CL^{pro}$ respectively, showing

the affinity that **3** has for the active site region including the catalytic residues. The hybrid **3** blocked the active site area of both proteases through hydrophobic interactions and H-bonding of the fullerene core and the androsterone moiety. The lowest binding energy obtained for the $3CL^{pro}$ is due to the higher number of H-bonds and residues interacting in comparison with PL^{pro} (See Figure 4.

SARS-Cov-2 proteases are essential enzymes in the process of coronavirus replication; hence, they have been a popular target for coronavirus inhibitors. From the generated docking model, the fullerene derivative **3** was bound in the active site of PL^{pro} interacting with ASN-157, LYS-158, GLU-162, GLU-168, HIS-172, TYR-269, and GLN-270 (Figure 5A). The binding sites of **3** are consistent with those of the crystalized inhibitor used as control and some antiviral drug docked.[61] A hydrogen bonding was predicted between the phenolic hydrogen atom of TYR-269 and the malonate linker group. Moreover, the aromatic region of this residue interacts with the fullerene core through T-shape and π–π interactions.[62]

It is have been determined that the $3CL^{pro}$ is the key protein during virus replication; its principal function is to hydrolyze the polymerase expressed by the virus so the occlusion of the SARS-Cov-2 protease ($3CL^{pro}$) active site inhibits the hydrolysis of the viral polymerase.[63] The active site of $3CL^{pro}$ is placed in the gap between the residues 8–101 and 102–184,[61] with HIS-41 and CYS-145 as catalytic residues.[64] The docking results show that THR-25, HIS-41, THR-45, SER-46, MET-49, ASN-142 HIS-144, CYS145, MET-165, and GLU-166 are the main interacting residues with compound **3** (See Figure 5B). The carbonyl group of the malonate linker forms hydrogen bonds with ASN-142 and GLU-166. The hydrogen bonds and hydrophobic interactions are consistent with those found in the crystalized inhibitor and the anti-asthmatic drug Montelukast.[61]

The binding energy study and the interaction with the active residues indicate that **3** has a potential use in anti-viral therapies against Covid-19.

On the other hand, a molecular docking simulation was also applied to the pristine $H_2@C_{60}$ to find the binding affinity with the enzymes PL^{pro} and $3CL^{pro}$ previously studied.

$H_2@C_{60}$ only shows hydrophobic interactions with both receptors, and the calculated binding energies were −10.0 kcal/mol and −10.2 kcal/mol for PL^{pro} and $3CL^{pro}$ respectively. The interlinkage with PL^{pro} does not match with the reported for **3** because it interacts with HIS-74, THR-75, LEU-76, ASP-77, GLN-175, and HIS-176 residues. These amino acids are not key residues in the enzyme inhibition, and consequently the endohedral fullerene is not considered a potential inhibitor for PL^{pro}. A different result was obtained for $3CL^{pro}$, because $H_2@C_{60}$ interacts with the main residues of the enzyme-like compound **3** but with lower affinity energy, since it cannot forms strong interactions through hydrogen bonds. Figure 6 shows the low-energy binding conformations of **3** and $H_2@C_{60}$ bound to human SARS-Cov-2 enzymes.

The binding energy study and the interaction with the active residues indicate that **3** has a higher potential use in anti-viral therapies against Covid-19. The functionalization of $H_2@C_{60}$ with a steroid moiety is a way to increase the biomolecular recognition areas and increase the strength of the union with the enzymatic receptors. These results must be verified by future *in vitro* and *in vivo* assays. Similar results were obtained with the previously reported empty steroid-C_{60}[31] because the

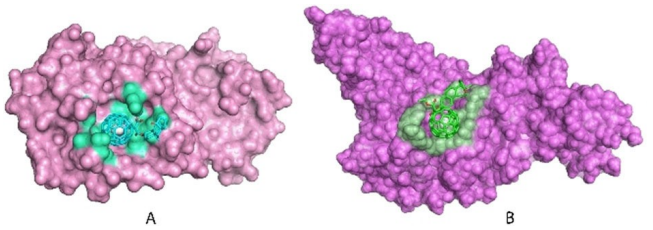

Figure 4. Low-energy binding conformations of **3** bound to human SARS-Cov-2 generated by molecular docking. The proteases are shown as an electrostatic surface model and the ligand is represented in sticks. The hydrogen molecule is represented in spheres. (A) Structure of PL^{pro}-fullerene hybrid complex. (B) Structure of $3CL^{pro}$-fullerene hybrid complex.

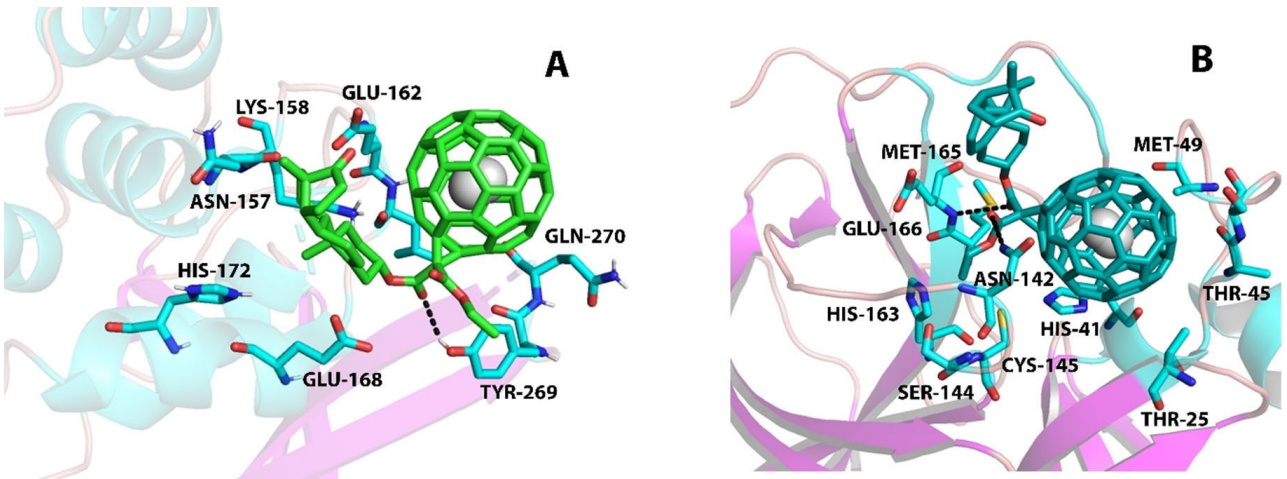

Figure 5. Low-energy binding conformations of 3 bound to human SARS-Cov-2 generated by molecular docking. The proteases are shown as an electrostatic surface model and the ligand is represented in sticks. The hydrogen molecule is represented in spheres. (A) Structure of PL^{pro}-fullerene hybrid complex. (B) Structure of $3CL^{pro}$-fullerene hybrid complex.

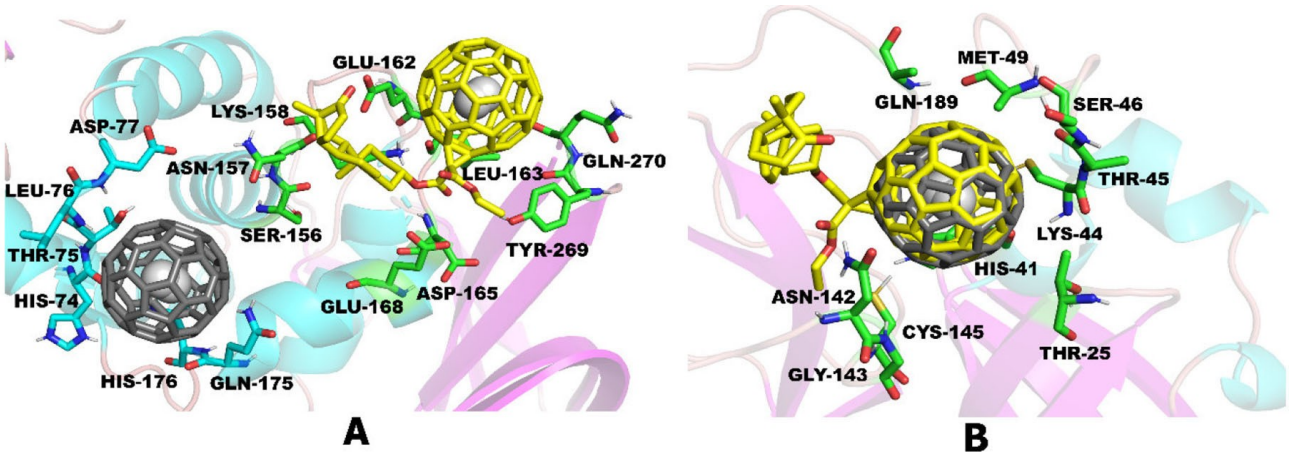

Figure 6. Low-energy binding conformations of **3** and $H_2@C_{60}$ bound to human SARS-Cov-2 enzymes generated by molecular docking. The proteases are shown in the cartoon model and the ligand is represented in sticks, $H_2@C_{60}$ in grey and **3** in yellow. The interacting residues (distance $\leq$0.4 nm) are represented in sticks and the hydrogen molecule was represented in spheres. A) Superimposed image of the $H_2@C_{60}$–PL^{pro} and hybrid **3**-PL^{pro} complexes in the active site. (B) Superimposed image of the $H_2@C_{60}$–$3CL^{pro}$ and hybrid **3**–$3CL^{pro}$ complexes in the active site.

fundamental interactions between the ligand and the proteases residues occur between the groups present in the malonate-steroid moiety (see Supporting Information Tables S8 and S9, Figures S16–S18).

Conclusion

In summary, the synthesis of $H_2@61$-(ethoxycarbonyl)-61-(3β-*O*-carbetoxy-5-androsten-17-one)methano[60]fullerene (**3**) has been performed using the Bingel-Hirsch protocol with a good yield. The reaction path is similar to that when pristine C_{60} is used. A comprehensive spectroscopic and analytical study confirmed the chemical structure of the new compound. Calculations have predicted that the cyclohexane ring A of the steroid moiety presents a chair conformation and the carbonyl groups in the malonate moiety shows an antiperiplanar disposition. Additionally, it was also possible to determine that in $H_2@C_{60}$, the hydrogen molecule does not present a clear perpendicular disposition to any of the hexagon rings of the fullerene cage. All theoretical physicochemical parameters were consistent with the structure of **3**, and allow us to infer the behavior of the novel hybrid in the environment of the biological fluids and its potential to traverse biological membranes. A binding energy study with the active residues of human SARS-Cov-2 enzymes and the interactions found indicate that the steroid-$H_2@C_{60}$ hybrid has potential for its implementation in further studies towards anti-viral therapies against SARS-Cov-2.

Experimental Section

General: All reagents were of commercial quality and were used as supplied unless otherwise specified. Solvents were dried by standard procedures. All reactions were performed using an atmosphere of argon and oven-dried glassware. Reactions were monitored by thin-layer chromatography carried out on 0.25 mm silica gel plates (230-400 mesh). Flash column chromatography was performed using silica gel (60 Å, 32–63 μm). ^{1}H NMR spectra were recorded at 700 MHz, and ^{13}C NMR at 175 MHz; the one-bond heteronuclear correlation (HMQC) and the long-range ^{1}H-^{13}C correlation (HMBC) spectra were obtained by use of the inv4gs and the inv4gslplrnd programs. HRMS were recorded under MALDI (dithranol as matrix) conditions in positive mode of detection. A high-performance liquid chromatography (HPLC) system (Cosmosil Buckyprep preparative column, dimensions, 4.6×250 mm^2; flow rate 1.0 mL min^{-1}, injection volume 15 μL, eluent toluene) was used to determine the purity of the compounds synthesized. The retention times (t_R) reported were determined at a wavelength of 320 nm. FTIR spectra were carried out using ATR of the solid compound. UV/Vis spectra were recorded in $CHCl_3$.

Computational methods: All molecules were built with Avogadro.[65] For the semi-empirical calculations MOPAC2016[66] was used, and DFT calculation was performed with ORCA 4.2.1.[66] All structures were pre-calculated using the semi-empirical PM6 method with dispersion correction D3H4 as a satisfactory starting point for large carbon structure, especially fullerene derivatives.[34] Then structures were optimized using Density Functional Theory at gradient-corrected exchange-correlation functional of Perdew, Burke, and Ernzerhof (PBE)[68] method using 6-31G(d) and refined with 6-311G(d,p) basis set as described somewhere else.[69] The Grimme in combination with the Becke-Johnson damping (D3BJ)[70] method for empirical dispersion corrections together with the contribution of three-body dispersion terms, was employed, as the long-range dispersion interactions in endohedral fullerene are very important to consider in both geometry optimizations. The coulomb part integration was solved using Resolution of Identity (RI) approximation (with def2/J auxiliary basis set as a keyword in ORCA). To avoid imaginary frequency modes (negative frequencies) together with numerical noise, the TightOpt with VeryThight convergence as keywords was employed. Improving the numerical precision as ORCA implantation permits. The Lebedev302 grid (Grid4) during the SCF iterations and Lebedev434 (Grid 5) as a final grid for the final energy evaluation after SCF convergence was set for integration precision.

The frontier orbitals HOMO/LUMO were visualized directly from the optimized structure with DFT/PBE quantum mechanical calculation with 6-311G(d,p) basis set using IboView v29150427[71] and this conformation was used for the calculation of dipole moment and

visualization of the electrostatic potential map. The Log P was calculate using XLOGP2v3.2.0.[48] For molecular electrostatic map first the mep.py python script written by Marius Retegan[72] was used for cube file preparation and then was visualized using VMD 1.9.3.[73] NCI analysis was performed using NCIPLOT 4.0[43] and the result visualized with VMD 1.9.3. For visualization of optimized structure, Mercury 2020.1 was used.[74] The DFT GIAO calculations were carried out on previously optimized structure at the TPSS level as this functional similar accuracy compares to hybrid functionals at much lower computational cost[75] together with NMR optimized triple ζ basis set namely pcSseg-2[76] with CPCM continuum solvation model using chloroform. The provided chemical shift are referenced to tetramethylsilane optimized and calculated using the same methodology as studied compounds.

Molecular Docking: *Ligand/Protein Preparation.* Ligand optimized structure was obtained with DFT PBE method. The structure of human Coronavirus proteases papain-like (PL^{pro}) [PDB ID: 4OVZ (R = 2.50 Å) chain A][57] and ($3CL^{pro}$) [PDB ID: 6LU7 (R = 2.02 Å) chain A)][58] were used as the model of SARS-Cov-2 proteins and downloaded from Protein Data Bank (PDB) (http://rcsb.org). The crystallized inhibitors were removed and used as control molecules. The proteins were processed by removing water, adding polar hydrogen atoms, and default rotatable bonds were retained. Ligands optimized structures were obtained with the DFT PBE method.[68] The Gasteiger model was used for the calculations of the partial charges of the ligands. The proteins and ligand structures were saved in PDBQT format with AutoDock Tools.[77] The center of the simulations were boxes of size (40 Å × 40 Å × 40 Å) centered at (−16.333, 42.889, −38.722) for the PL^{pro} and (50 Å × 50 Å × 50 Å) centered at (−60.039, −38.173, 26.194) for the $3CL^{pro}$.

Molecular Docking Simulation and Analysis of Target-Ligand Complexes. Molecular docking between the proteins and the ligand was performed using AutoDock Vina 1.1.2.[78] Docking parameters were set to default, except for *exhaustiveness* = 32 and *num_modes* = 2. Ten independent runs were performed in each case, and the two best-docked conformations of each run were analyzed, according to the affinity calculated with the scoring function. The total docked conformations were grouped based upon *Root Mean Square Deviation* (RMSD) of the different bound poses. The RMSD difference between conformations of the same cluster was set to less than 2 Å. The binding free energy (kcal/mol) of every cluster was calculated as the mean binding free energy (MBFE) of all the conformations present in the same cluster. The cluster 3D structures of the representative binding mode for each complex with best-scoring pose were represented using PyMOL 2.1.0.[79]

Synthesis and Characterization

Synthesis of 3β-ethylmalonate-5-androsten-17-one (1): This compound was prepared by following the method previously reported by us.[31]

Synthesis of H_2@61-(ethoxycarbonyl)-61-(3β-*O*-carbetoxy-5-androsten-17-one)methano [60]fullerene (3): To a solution of $H_2@C_{60}$ (30 mg, 0.041 mmol) in dry toluene (50 mL) was added 3β-ethyl malonate-5-androsten-17-one (**1**, 21 mg, 0.053 mmol), CBr_4 (18 mg, 0.053 mmol), and diazabicyclo[4.2.0]undec-7-ene (DBU; 0.1 mL, 0.67 mmol) in that order. The reaction mixture was then stirred at room temperature for 3 h under argon atmosphere. The color of the solution changed from purple to brown. Water was added, and the residue was extracted with toluene. The organic layer was dried over $MgSO_4$, filtered, and concentrated *in vacuo*. The crude product was purified by column chromatography on silica gel, first with CS_2 to elute unreacted C_{60} and finally with dichloromethane. With characterization purposes, additional purification of these compounds was carried out by repetitive precipitation and centrifugation using hexane, methanol, and diethyl ether as solvents. Chemical yield: 76% (35 mg, 0.031 mmol), amorphous brown solid. HPLC: toluene:acetonitrile, 9:1, flow rate 1 mL/min, t_R = 5.5 min. ^{1}H NMR (700 MHz, $CDCl_3$, δ ppm): 5.52 (d, *J* = 5.1 Hz, 1H, H6), 5.03 (m, 1H, H3), 4.58 (q, *J* = 7.1 Hz, 2H, CH_2O), 2.58 (m, 2H, H1), 2.48 (dd, *J* = 19.2 Hz, *J* = 8.7 Hz, 1H, H16), 2.17 (m, 1H, H12), 2.13 (m, 1H, H2), 2.10 (m, 1H, H16), 1.98 (m, 1H, H4), 1.97 (m, 1H, H15), 1.88 (m, 1H, H7), 1.84 (m, 1H, H2), 1.72 (m, 1H, H11), 1.70 (m, 1H, H8), 1.58 (m, 1H, H15), 1.55 (m, 1H, H11), 1.51 (t, *J* = 7.1 Hz, 3H, CH_3CH_2), 1.35 (m, 1H, H14), 1.32 (m, 1H, H7), 1.27 (m, 1H, H12), 1.25 (m, 1H, H4), 1.12 (s, 3H, CH_3–C10), 1.09 (m, 1H, H9), 0.91 (s, 3H, CH_3–C13), −3.13 (s, 2H, H_2) ^{13}C{1H} NMR (175 MHz, $CDCl_3$, δ ppm): 221.2 (C17), 163.8 (C=O), 163.1 (C=O), 145.51, 145.47, 145.42, 145.1, 144.9, 144.8, 144.12, 144.11, 143.33, 143.25, 143.22, 143.17, 142.5, 142.12, 142.10, 141.2, 139.48, 139.46, 139.2 (C5), 122.9 (C6), 77.4 (C3), 72.7 (Csp^3 cyclopropane ring), 71.8 (Csp^3 cyclopropane ring), 63.5 (CH_2O), 52.5 (C61 cyclopropane ring), 51.8 (C14), 50.3 (C9), 47.7 (C13), 38.0 (C1), 37.0 (C4), 36.9 (C10), 36.0 (C16), 31.6 (C8), 31.5 (C7), 31.0 (C12), 27.8 (C2), 22.0 (C15), 20.5 (C11), 19.6 (CH_3–C10), 14.5 (CH_3CH_2), 13.7 (CH_3–C13). ATR-FTIR: ν 2930, 2864, 1720 (C=O), 1665, 1614, 1453, 1376, 1265, 1226, 1181, 1118, 1020, 730 cm^{-1}. HRMS (MALDI-TOF): *m/z*: M^+ Calcd for $C_{84}H_{34}O_5$: 1122.2406; Found 1122.2399.

Acknowledgements

Financial support by the Ministerio de Economía y Competitividad (MINECO) of Spain (project CTQ2017-83531-R), PNCB of MES, Cuba (P223LH-001-059), and Yachay Tech. internal Project Theoretical and Morphological studies are acknowledged.

Conflict of Interest

The authors declare no conflict of interest.

Keywords: cyclopropanation · fullerenes · molecular docking · SARS-Cov-2 · steroid hybrids

[1] K. Kurotobi, Y. Murata, *Science* **2011**, *333*, 613–616.
[2] a) R. Beyers, C.-H. Kiang, R. D. Johnson, J. R. Salem, M. S. De Vries, C. S. Yannoni, D. S. Bethune, H. C. Dorn, P. Burbank, K. Harichi, S. Stevenson, *Nature* **1994**, *370*, 196–199; b) M. N. Chaur, F. Melin, A. L. Ortíz, L. Echegoyen, *Angew. Chem. Int. Ed.* **2009**, *48*, 7514–7538; *Angew. Chem.* **2009**, *121*, 7650–7675.
[3] S. Stevenson, G. Rice, T. Glass, K. Harich, F. Cromer, M. R. Jordan, J. Craft, E. Hadjun, R. Bible, M. M. Olmstead, K. Maitra, A. J. Fischer, A. L. Balch, H. C. Dorn, *Nature* **1999**, *401*, 55–57.
[4] D. W. Cagle, S. J. Kennel, S. Mizadeth, J. M. Alford, L. J. Wilson, *Proc. Natl. Acad. Sci. USA* **1999**, *96*, 5182–5187.
[5] a) P. P. Fatouros, F. D. Corwin, Z.-J. Chen, W. C. Broaddus, J. L. Tatum, B. Kettenman, Z. Ge, H. W. Gibson, J. L. Russ, A.-P. Leonard, J. C. Duchamp, H. C. Dorn, *Radiology* **2006**, *240*, 756–764; b) J. Zhang, P. P. Fatouros, C. Shu, J. Reid, L. S. Owens, T. Cai, H. W. Gibson, G. L. Long, F. D. Corwin, Z.-J. Chen, H. C. Dorn, *Bioconjugate Chem.* **2010**, *21*, 610–615.
[6] a) S. Kobayashi, S. Mori, S. Iida, H. Ando, T. Takenobu, Y. Taguchi, A. Fujiwara, A. Taninaka, H. Shinohara, Y. Iwasa, *J. Am. Chem. Soc.* **2003**, *125*, 8116–8117; b) Y. Yasutake, Z. Shi, T. Okazaki, H. Shinohara, Y. Majima, *Nano Lett.* **2005**, *5*, 1057–1060.
[7] T. Tsuchiya, R. Kumashiro, K. Tanigaki, Y. Matsunaga, M. O. Ishitsuka, T. Wakahara, Y. Maeda, Y. Takano, M. Aoyagi, T. Akasaka, M. T. H. Liu, T. Kato, K. Suenaga, J. S. Jeong, S. Ijima, F. Kimura, T. Kimura, S. Nagase, *J. Am. Chem. Soc.* **2008**, *130*, 450–451.

[8] Y. Rubin, *Top. Curr. Chem.* **1999**, *199*, 67–91.
[9] Y. Murata, M. Murata, K. Komatsu, *J. Am. Chem. Soc.* **2003** *125*, 7152–7153.
[10] a) K. Komatsu, M. Murata, Y. Murata, *Science* **2005**, *307*, 238–240; b) M. Murata, Y. Murata, K. Komatsu, *J. Am. Chem. Soc.* **2006**, *128*, 8024–8033.
[11] A. Krachmalnicoff, M. H. Levitt, R. J. Whitby, *Chem. Commun.* **2014**, *50*, 13037–13040.
[12] L. Ga, *Acc. Chem. Res.* **2019**, *52*, 1793–1801.
[13] a) T. Rõõm, L. Peedu, Min Ge, D. Hüvonen, U. Nagel, Shufeng Ye, Minzhong Xu, Z. Basic, S. Mamone, M. H. Levitt, M. Carravetta, J. Y.-C. Chen, Xuegong Lei, N. J. Turro, Y. Murata, K. Komatsu, *Philos. Trans. R. Soc. London Ser. A* **2013**, 371, 20110631, and references given therein; b) S. Mamone, J. Y. C. Chen, R. Bhattacharyya, M. H. Levitt, R. G. Lawler, A. J. Horsewill, T. Rõõm, Z. Bacic, N. J. Turro, *Coord. Chem. Rev.* **2011**, *255*, 938–948.
[14] a) M. Murata, Y. Ochi, F. Tanabe, K. Komatsu, Y. Murata, *Angew. Chem. Int. Ed.* **2008**, *47*, 2039–2041; *Angew. Chem.* **2008**, *120*, 2069–2071; b) K. Kouril, C. Wickens, B. Meier, S. Alom, J. Grasvik, R. J. Whitby, M. H. Levitt, *Phys. Chem. Chem. Phys.* **2017**, *191*, 11793–11801.
[15] M. Ya. Amusia, L. V. Chernysheva, S. K. Semenov, *JETP Lett.* **2019**, *110*, 102–106.
[16] a) C.-K. Yang, *Carbon* **2007**, *45*, 2445–2458; b) G. Jimenez-Osés, J. I. García, F. Corzana, J. Elguero, *Org. Lett.* **2011**, *13*, 2528–2531; c) G. A. Dolgonos, G. H. Peslherbe, *Phys. Chem. Chem. Phys.* **2014**, *16*, 26294–26305; d) S. Mamone, M. Jimenez-Ruiz, M. R. Johnson, S. Rols, A. J. Horsewill, *Phys. Chem. Chem. Phys.* **2016**, *18*, 29369–29380.
[17] Y. Li, X. Lei, R. G. Lawler, Y. Murata, K. Komatsu, N. J. Turro, *J. Phys. Chem. Lett.* **2010**, *1*, 2135–2138.
[18] Y. Li, X. Lei, R. G. Lawler, Y. Murata, K. Komatsu, N. J. Turro, *J. Phys. Chem. Lett.* **2011**, *2*, 741–744.
[19] Y. Li, X. Lei, X. Li, R. G. Lawler, Y. Murata, K. Komatsu, N. J. Turro, *Chem. Commun.* **2011**, *47*, 12527–12529.
[20] L. Garbuio, Y. Li, S. Antonello, J. A. Gascón, R. G. Lawler, X. Lei, Y. Murata, N. J. Turro, F. Maran, *Photochem. Photobiol.* **2014**, *90*, 439–447.
[21] Y. Li, X. Lei, R. G. Lawler, Y. Murata, K. Komatsu, N. J. Turro, *Chem. Commun.* **2011**, *47*, 2282–2284.
[22] E. E. Maroto, M. Izquierdo, M. Murata, S. Filippone, K. Komatsu, Y. Murata, N. Martín, *Chem. Commun.* **2014**, *50*, 740–742.
[23] a) S. Filippone, E. E. Maroto, A. Martín-Domenech, M. Suárez, N. Martín, *Nat. Chem.* **2009**, *1*, 578–582; b) E. E. Maroto, A. de Cózar, S. Filippone, A. Martín-Domenech, M. Suárez, F. P. Cossió, N. Martín, *Angew. Chem. Int. Ed.* **2011**, *50*, 6060–6064; *Angew. Chem.* **2011**, *123*, 6184–6188; c) E. E. Maroto, S. Filippone, A. Martín-Domenech, M. Suárez, N. Martín, *J. Am. Chem. Soc.* **2012**, *134*, 12936–12938; d) E. E. Maroto, S. Filippone, M. Suarez, R. Martinez-Alvarez, A. de Cozar, F. P. Cossio, N. Martin, *J. Am. Chem. Soc.* **2014**, *136*, 705–712.
[24] J. Lopez-Gejo, A. A. Martí, M. Ruzzi, S Jocksch, K. Komatsu, F. Tanabe, Y. Murata, N. J. Turro, *J. Am. Chem. Soc.* **2007**, *129*, 14554–14555.
[25] a) J. Coro, H. Rodríguez, D. G. Rivera, M. Suárez, D. Molero, M. A. Herranz, R. Martínez-Álvarez, S. Filippone, N. Martín, *Eur. J. Org. Chem.* **2009**, *2009*, 4810–4817; b) A. Ruiz, J. Coro, L. Almagro, J. A. Ruiz, D. Molero, E. E. Maroto, S. Filippone, M. A. Herranz, R. Martinez-Alvarez, J. C. Sancho Garcia, F. Di Meo, M. Suárez, N. Martín, *J. Org. Chem.* **2013**, *78*, 2819–2826; c) A. Ruiz, C. Morera-Boado, L. Almagro, J. Coro, E. E. Maroto, M. A. Herranz, S. Filippone, D. Molero, R. Martinez-Alvarez, J. M. Garcia de la Vega, M. Suárez, N. Martín, *J. Org. Chem.* **2014**, *79*, 3473–3486; d) M. Suarez, A. Ruiz, L. Almagro, J. Coro, E. E. Maroto, S. Filippone, D. Molero, R. Martinez-Alvarez, N. Martin, *J. Org. Chem.* **2017**, *82*, 4654–4660; e) L. Almagro, D. Hernandez-Castillo, O. Ortiz, D. Alonso, A. Ruiz, J. Coro, M. A. Herranz, D. Molero, R. Martinez-Alvarez, M. Suarez, N. Martín, *Eur. J. Org. Chem.* **2018**, *2018*, 4512–4522; f) D. Alonso, D. Hernandez-Castillo, L. Almagro, R. Gonzalez-Aleman, D. Molero, M. A. Herranz, E. Medina-Paez, J. Coro, R. Martinez-Alvarez, M. Suarez, N. Martin, *J. Org. Chem.* **2020**, *85*, 2426–2437.
[26] a) W. L. Miller, R. J. Auchus, *Endocr. Rev.* **2011**, 32, 81–151; b) E. Friess, T. Schiffelholz, T. Steckler, A. Steiger, *Eur. J. Clin. Invest.* **2000**, *30*, 46–50; c) L. E. Kihel, *Steroids* **2012**, *77*, 10–26.
[27] C. Bingel, *Chem. Ber.* **1996**, *26*, 1957–1959.
[28] M. T. ul Qamar, S. M. Alqahtani, M. A. Alamri, L–L. Chen, *J. Pharm Anal.* **2020**, *10*, 313–319.
[29] J.-Y. Park, J.-A. Ko, D. W. Kim, Y. M. Kim, H.-J. Kwon, H. J. Jeong, C. Y. Kim, K. H. Park, W. S. Lee, Y. B. Ryu, *J. Enzyme Inhib. Med. Chem.* **2016**, *31*, 1, 23–30.
[30] Y. Chen, Q. Zhang, D. Guo, *J. Med. Virol.* **2020**, *92*, 418–323.
[31] L. Almagro, R. Lemos, K. Makowski, H. Rodríguez, O. Ortiz, W. Cáceres, M. Á. Herranz, D. Molero, R. Martínez-Álvarez, M. Suárez, N. Martín, *Eur. J. Org. Chem.* **2020**, *2020*, 5926–5937.
[32] A. Bianco, M. Maggini, G. Scorrano, C. Toniolo, G. Marconi, C. Villani, M. Prato, *J. Am. Chem. Soc.* **1996**, *118*, 4072–4080.
[33] C. Du, J. Xu, Y. Li, W. Xu, D. Zhu, *Chin. Sci. Bull.* **2001**, *46*, 1156–1159.
[34] C. Sikorska, T. Puzyn, *Nanotechnology* **2015**, *26*, 455702.
[35] H. Wang, Y. He, Y. Li, H. Su, *J. Phys. Chem. A* **2012**, *116*, 255–262.
[36] H. Kruse, S. Grimme, *J. Phys. Chem. C* **2009**, *113*, 17006–17010.
[37] V. V. Kuznetsov, *Russ. J. Gen. Chem.* **2013**, *83*, 1163–1164.
[38] G. A. Dolgonos, *Carbon* **2008**, *46*, 704–705.
[39] S. Grimme, S. Ehrlich, L. Goerigk, *J. Comput. Chem.* **2011**, *32*, 1456–1465.
[40] T. Korona, A. Hesselmann, H. Dodziuk, *J. Chem. Theory Comput.* **2009**, *5*, 1585–1596.
[41] R. J. Cross, *J. Phys. Chem. A* **2001**, *105*, 6943–6944.
[42] E. R. Johnson, S. Keinan, P. Mori-Sánchez, J. Contreras-García, A. J. Cohen, W. Yang, *J. Am. Chem.* **2010**, *132*, 6498–6506.
[43] a) R. Boto, F. Peccati, R. Laplaza, A. Carbone, J.-P. Piquemal, Y. Maday, J. Contreras-García, *NCIPLOT4*, **2020**; b) J. Contreras-García, E. Johnson, S. Keinan, R. Chaudret, J. Piquemal, D. Beratan, W. Yang, *J. Chem. Theory Comput.* **2011**, *7*, 625–632.
[44] C. N. Ramachandran, D. Roy, N. Sathyamurthy, *Chem. Phys. Lett.* **2008**, *461*, 87–92.
[45] M. F. Sanner, A. J. Olson, J. C. Spehner, *Biopolymers* **1996**, *38*, 305–320.
[46] S. Mitternacht, *F1000Research* **2016**, *5*, 189.
[47] J. Dong, Z.-J. Yao, M. Wen, M.-F. Zhu, N.-N. Wang, H.-Y. Miao, A.-P. Lu, W.-B. Zeng, D.-S. Cao, *J. Cheminf.* **2016**, *8*, 34.
[48] T. Cheng, Y. Zhao, X. Li, F. Lin, Y. Xu, X. Zhang, Y. Li, R. Wang, L. Lai, *J. Chem. Inf. Model.* **2007**, *47*, 2140–2148.
[49] M. Calvaresi, S. Furini, C. Domene, A. Bottoni, F. Zerbetto, *ACS Nano* **2015**, *9*, 4827–4834.
[50] K. Palm, P. Stenberg, K. Luthman, P. Artursson, *Pharm. Res.* **1997**, *14*, 568–571.
[51] Y. Kawano, T. Kondo, *Chem. Lett.* **2014**, *43*, 483–485.
[52] C. T. Jafvert, P. P. Kulkarni, *Environ. Sci. Technol.* **2008**, *42*, 5945–5950.
[53] Z.-H. Tong, M. Bischoff, L. F. Nies, N. J. Carroll, B. Applegate, R. F. Turco, *Sci. Rep.* **2016**, *6*, 1–9.
[54] N. O. Mchedlov-Petrossyan, *Theor. Exp. Chem.* **2020**, *55*, 361–391.
[55] M. E. Pérez-Ojeda, I. Wabra, C. Böttcher, A. Hirsch, *Chem. Eur. J.* **2018**, *24*, 14088–14100.
[56] A. V. Marenich, C. J. Cramer, D. G. Truhlar, *Chem. Sci.* **2013**, *4*, 2349–2356.
[57] Y. M. Báez-Santos, S. J. Barraza, M. W. Wilson, M. P. Agius, A. M. Mielech, N. M. Davis, S. C. Baker, S. D. Larsen, A. D. Mesecar, *J. Med. Chem.* **2014**, *57*, 2393–2412.
[58] Z. Jin, X. Du, Y. Xu, Y. Deng, M. Liu, Y. Zhao, B. Zhang, X. Li, L. Zhang, C. Peng, Y. Duan, J. Yu, L. Wang, K. Yang, F. Liu, R. Jiang, X. Yang, T. You, X. Liu, X. Yang, F. Bai, H. Liu, X. Liu, L. W. Guddat, W. Xu, G. Xiao, C. Qin, Z. Shi, H. Jiang, Z. Rao, H. Yang, *Nature* **2020**, *582*, 289–293.
[59] R. Yu, L. Chen, R. Lan, R. Shen, P. Li, *Int. J. Antimicrob. Agents* **2020**, *56*, 106012.
[60] P. A. Borea, K. Varani, S. Gessi, P. Gilli, A. Dalpiaz, *Il Farmaco* **1998**, *53*, 249–254.
[61] C. Wu, Y. Liu, Y. Yang, P. Zhang, W. Zhong, Y. Wang, Q. Wang, Y. Xu, M. Li, X. Li, M. Zheng, L. Chen, H. Li, *Acta Pharm. Sin. B* **2020**, *10*, 766–788.
[62] A. Barzegar, E. Naghizadeh, M. Zakariazadeh, J. Azamat, *Mini-Rev. Med. Chem.* **2017**, *17*, 633–647.
[63] D Hu, C. Shao, W. Guan, Z. Su, J. Sun, *J. Inorg. Biochem.* **2007**, *101*, 89–94.
[64] H. Yang, M. Yang, Y. Ding, Y. Liu, Z. Lou, Z. Zhou, L. Sun, L. Mo, S. Ye, H. Pang, G. F. Gao, K. Anand, M. Bartlam, R. Hilgenfeld, Z. Rao, *Proc. Natl. Acad. Sci. USA.* **2003**, *100*, 13190–13195.
[65] M. D. Hanwell, D. E. Curtis, D. C. Lonie, T. Vandermeersch, E. Zurek, G. R. Hutchison, *J. Cheminf.* **2012**, *4*, 17.
[66] J. J. P. Stewart, *MOPAC2016* **2016**.
[67] F. Neese, F. Wennmohs, U. Becker, C. Riplinger, *J. Chem. Phys.* **2020**, *152*, 224108.
[68] J. P. Perdew, K. Burke, M. Ernzerhof, *Phys. Rev. Lett.* **1997**, *78*, 1396.
[69] H. Wang, Y. He, Y. Li, H. Su, *J. Phys. Chem. A* **2012**, *116*, 255–262.
[70] S. Grimme, S. Ehrlich, L. Goerigk, *J. Comput. Chem.* **2011**, *32*, 1456–1465.
[71] G. Knizia, J. E. M. N. Klein, *Angew. Chem. Int. Ed.* **2015**, *54*, 5518–5522; *Angew. Chem.* **2015**, *127*, 5609–5613.
[72] M. Retegan, *Mep.Py.* **2019**, https://gist.github.com/mretegan/5501553#file-mep-py.
[73] W. Humphrey, A. Dalke, K. Schulten, *J. Mol. Graphics* **1996**, *14*, 33–38.

[74] C. F. Macrae, I. Sovago, S. J. Cottrell, P. T. A. Galek, P. McCabe, E. Pidcock, M. Platings, G. P. Shields, J. S. Stevens, M. Towler, P. A. Wood, *J. Appl. Crystallogr.* **2020**, *53*, 226–235.
[75] G. L. Stoychev, A. A. Auer, F. Neese, *J. Chem. Theory Comput.* **2018**, *14*, 4756–4771.
[76] F. Jensen, *J. Chem. Theory Comput.* **2015**, 11, 132–138.
[77] M. F. Sanner, *J. Mol. Graphics Modell.* **1999**, *17*, 57–61.
[78] O. Trott, A. J. Olsonm, *J. Comb. Chem.* **2010**, *31*, 455–461.
[79] L. L. C. Schrodinger, *The PyMOL Molecular Graphics System*, Version 2.1.0.

Manuscript received: December 2, 2020
Revised manuscript received: January 21, 2021
Accepted manuscript online: January 22, 2021